Scattering-theoretic approach to the electronic structure of semiconductor surfaces: The (100) surface of tetrahedral semiconductors and SiO_2

J. Pollmann* and Sokrates T. Pantelides
IBM Thomas J. Watson Research Center, Yorktown Heights, New York 10598
(Received 30 May 1978)

We report the development of a method for calculating the electronic structure of semiconductor surfaces. It is based on the Koster-Slater idea for treating localized perturbations, which was later extended to describe surfaces. The present method makes use of semiempirical tight-binding Hamiltonians and of a novel way to create free surfaces. A Green's-function scattering-theoretical formulation is employed. The properties of the bulk crystal are built in and preserved. Bound-surface-state energies are determined unambiguously and accurately even for states whose wave functions are very extended. The total and local changes occurring in the density of states due to the surface can be calculated directly, and therefore very accurately, without having to subtract two large quantities. Some of the structure in the state-density changes is in the form of narrow peaks, which can be identified as resonances or antiresonances. In order to point out advantages of the method and to compare our results with the results of slab calculations, we present applications to the Si and Ge (100) free surfaces. The present method is shown to be very efficient, accurate, and fast. Despite the fact that a tight-binding Hamiltonian of a truly semi-infinite system is treated exactly, the method employs matrices which are much smaller than those arising in slab calculations. Finally, the method is applied to a study of the (100) surfaces of the isoelectronic series Ge-GaAs-ZnSe and to the (100) surfaces of cubic SiO_2.

I. INTRODUCTION

The problem of the electronic structure of solid surfaces has attracted considerable attention during the last several years.[1-6] A variety of methods have been developed and used to study surfaces of metals and semiconductors. These methods belong to one of four general categories: (a) methods that simulate the semi-infinite solid with a finite number of atoms[7-10] (cluster methods); (b) methods that simulate the semi-infinite solid with a finite number of atomic layers having two-dimensional periodicity[11-24] (slab methods); (c) methods that solve the Hamiltonian of the semi-infinite crystal directly (wave-function-matching method[25-28]; Green's-function-matching method[29-35]; transfer-matrix or continued-fraction method[36-42]); and (d) methods that treat the creation of a surface as a perturbation of an otherwise perfect infinite solid.[43-53] All the above methods may be used with a variety of one-electron Hamiltonians (semiempirical, Hartree-Fock, self-consistent pseudopotential, etc.) together with one of many possible basis sets in terms of which the wave functions are expanded (plane waves, atomic orbitals, muffin-tin orbitals, etc.)

All four classes of methods have been used widely in studies of ideal model systems as well as studies of real materials. For semiconductors, calculations have thus far been done in terms of only the first three classes of methods. Methods belonging to the fourth class, i.e., those treating the creation of a surface as a perturbation of the otherwise infinite perfect crystal, have been formulated by several authors,[43-53] in all cases making use of Green's functions. Applications have been mainly on ideal systems that simulate no real material and on the so-called jellium model used to simulate simple metals.[54,55] More recently, limited applications of such methods have been reported for surface states of some transition metals.[50,52]

In this paper we develop a method which treats the creation of a surface as a perturbation and is particularly suited for semiconductors and insulators. Its foundations are the same as those of the methods used or discussed in Refs. 43–55, in that it is based on a Green's-function formulation of scattering theory. It therefore has a number of distinct advantages. It deals with a truly semi-infinite solid, instead of a finite cluster of atoms or finite number of layers. As a consequence, the band continua are described in terms of continuous functions, instead of being simulated by a set of discrete states. Furthermore, the *changes* produced in the electronic structure of the infinite solid by the creation of the free surface are obtained directly, thereby avoiding the subtraction of two large quantities. From the computational point of view, it deals with matrices whose size is determined by the range of the potential change due to the surface. In contrast, cluster and slab methods deal with matrices whose size is determined by the range of surface-state wave functions, which is almost always considerably larger.

In our particular formulation, a linear-combination-of-atomic-orbitals (LCAO) representation is used as in Refs. 43–45 and 47–53 but a novel way of creating the surface is introduced, which allows the surface perturbation to be represented by very small matrices. More specifically, the matrices encountered in our method are usually an order of magnitude smaller than corresponding slab matrices.

The plan of this paper is as follows. In Sec. II we give the general results of scattering theory in solids, as it has been developed by Callaway,[56] Garcia-Moliner,[57] and others, and give the general form of the equations in a LCAO representation. The equations are then specialized for perturbations which, like surfaces, have two-dimensional periodicity. Finally, the form of the perturbation which corresponds to the creation of a surface is described and the method of calculation is discussed. In Sec. III we present applications of the method to the Si and Ge (100) surfaces using the same Hamiltonian employed by Pandey and Phillips[13,58] in slab calculations in order to make a direct comparison and demonstrate the power of the present method to describe real materials. In Sec. IV we apply the method to a study of the (100) surfaces of the isoelectronic series Ge-GaAs-ZnSe and of SiO_2. We end with the conclusions in Sec. V. Details of the calculations are given in a series of appendixes.

II. SCATTERING-THEORETIC FORMALISM

A. General results

Let H^0 be a one-electron Hamiltonian describing an infinite periodic solid. The corresponding eigenvalue problem,

$$H^0 \psi^0_{n\vec{k}} = E^0_{n\vec{k}} \psi^0_{n\vec{k}} , \tag{1}$$

yields the energy bands $E^0_{n\vec{k}}$ and the corresponding Bloch functions $\psi^0_{n\vec{k}}$. The one-particle Green's function G^0 of this system is defined for outgoing waves by

$$G^0(E) = \lim_{\epsilon \to 0^+} \frac{1}{E + i\epsilon - H^0} = \frac{1}{E^+ - H^0} , \tag{2}$$

where the superscript (+) on E in the second form is a short-hand notation for the full expression involving the limit as $\epsilon \to 0$ from above. The operator G^0 can also be conveniently expressed in terms of the complete set of Bloch eigensolutions of H^0 as

$$G^0(E) = \sum_{n\vec{k}} \frac{|\psi^0_{n\vec{k}}\rangle \langle \psi^0_{n\vec{k}}|}{E^+ - E^0_{n\vec{k}}} . \tag{3}$$

As usual, the density of states of H^0 is given by

$$N^0(E) = -(1/\pi)\,\mathrm{Im}\,\mathrm{Tr}\,G^0(E) . \tag{4}$$

Now let U be any perturbation, and let

$$H = H^0 + U \tag{5}$$

be the new one-electron Hamiltonian for the perturbed system. The new eigenvalue problem is

$$(H^0 + U)\psi = E\psi , \tag{6}$$

and the solutions fall into two categories: states with energies within the forbidden gaps of the spectrum of H^0, and states within the band continua. One therefore usually seeks to determine the positions of the discrete states in the band gaps and the changes produced in the density of states within the band continua.

For states in the band gaps one can immediately rewrite (6) in the form

$$(1 - G^0 U)\psi = 0 . \tag{7}$$

If ψ is expanded in terms of an orthonormal basis set ϕ_α, i.e.,

$$\psi = \sum_\alpha c_\alpha \phi_\alpha , \tag{8}$$

Equation (7) can be transformed to a set of linear algebraic equations for c_α

$$\sum_\beta \left(\delta_{\alpha\beta} - \sum_\gamma G^0_{\alpha\gamma}(E)\, U_{\gamma\beta} \right) c_\beta = 0 , \tag{9}$$

where the Green's function in the $\{\phi_\alpha\}$ representation is directly obtained from Eq. (3):

$$G^0_{\alpha\beta}(E) = \sum_{n\vec{k}} \frac{\langle \phi_\alpha | \psi^0_{n\vec{k}} \rangle \langle \psi^0_{n\vec{k}} | \phi_\beta \rangle}{E^+ - E^0_{n\vec{k}}} . \tag{10}$$

From Eq. (9), bound states correspond to zeros of the determinant

$$D(E) = \det \left\| \delta_{\alpha\beta} - \sum_\gamma G^0_{\alpha\gamma}(E)\, U_{\gamma\beta} \right\| . \tag{11}$$

An important feature of this result is that the effective order of the determinant in Eq. (11) is equal to the order of the matrix U, so that the method is particularly suitable for short-range perturbations. The scattering-theoretical aspect of this approach is quite obvious in that, in more formal terms, Eq. (11) actually determines the discrete poles of the scattering matrix. The process under consideration here is, of course, the scattering of Bloch waves by the perturbation potential creating the surface.

Once the bound-state energy is determined from Eq. (11), the corresponding wave function is calculated from Eq. (9).

The change in the density of states $\Delta N(E) = N(E) - N^0(E)$ within the bands is obtained by first defining the Green's function $G(E)$ for the

perturbed system by

$$G(E)=1/(E^{+}-H), \tag{12}$$

and relating it to $G^0(E)$ by Dyson's equation, i.e.,

$$G=G^0+G^0UG. \tag{13}$$

The new density of states is given by

$$N(E)=-(1/\pi)\,\mathrm{Im}\,\mathrm{Tr}G(E). \tag{14}$$

The change in the density of states $\Delta N(E)$ can now be conveniently written

$$\Delta N(E)=\frac{1}{\pi}\frac{d\delta(E)}{dE}, \tag{15}$$

where the quantity $\delta(E)$ is the phase shift, given by

$$\delta(E)=-\tan^{-1}[\mathrm{Im}\,D(E)/\mathrm{Re}\,D(E)], \tag{16}$$

where $D(E)$ is as defined by Eq. (11). It should be noted that $\Delta N(E)$ depends only on G^0 and U, so that its evaluation does not require the solution of Dyson's equation (13). Equation (16) shows that $\delta(E)$ goes through an odd multiple of $\frac{1}{2}\pi$ every time $\mathrm{Re}\,D(E)=0$. If such an energy is labeled E_0, one may then expand $D(E)$ in the vicinity of E_0 to obtain the corresponding contribution to the change in the density of states in a Lorentzian form centered at E_0:

$$\Delta N(E)=(\Gamma/2\pi)\{1/[(E-E_0)^2+\tfrac{1}{4}\Gamma^2]\}, \tag{17}$$

with the half width Γ given by

$$\Gamma=2\,\mathrm{Im}\,D(E_0)/\mathrm{Re}\,D'(E_0). \tag{18}$$

In (18), the prime denotes differentiation with respect to energy. When $\Gamma>0$, $\Delta N(E)$ corresponds to a resonance of half width Γ, whereas when $\Gamma<0$, $\Delta N(E)$ corresponds to an antiresonance with half width $|\Gamma|$. Note that the same expressions apply within the gaps where $\mathrm{Im}\,D(E)=0$ so that $\Gamma=0$ and Eq. (17) reduces to a δ function indicating a discrete state.

$\Delta N(E)$ satisfies the important sum rule

$$\int_{-\infty}^{\infty}dE\,\Delta N(E)=0, \tag{19}$$

known as Levinson's theorem. When the discrete states in the gaps are counted separately, (19) becomes

$$\int_{\text{bands}}dE\,\Delta N(E)=-N_b, \tag{20}$$

where N_b is the number of discrete states in the gaps.

The relation for the discrete states, Eq. (9), as it applies to point defects in semiconductors was first derived by Koster and Slater.[59] A more general treatment has been given by Callaway[56] and by Garcia-Moliner.[57] Callaway employed Wannier functions for the set ϕ_α, which are convenient for general analytical results but very cumbersome for actual calculations. More recently, the problem was formulated in terms of LCAO basis sets in the above fashion by Bernholc and Pantelides,[60] who used the method to calculate the electronic structure of the vacancy in several semiconductors. Here, we turn to surface-related problems and study an arbitrary perturbation that retains two-dimensional periodicity. Before we proceed further, however, we must introduce some necessary LCAO terminology.

B. LCAO representation—Planar perturbations

In order to describe a perfect infinite crystal in an LCAO representation, we introduce atomiclike orbitals on each atom in the primititive unit cell and denote them by $\varphi_\alpha(\vec{r}-\vec{\tau}_\nu)$, where $\vec{\tau}_\nu$ are the positions of the atoms in the unit cell and α labels the s, p, ..., etc., character of the orbitals. For the purpose of solving for the eigensolutions of H^0 we first define the Bloch sums

$$\chi_{\vec{k}}^{\alpha\nu}(\vec{r})=\frac{1}{\sqrt{N_3}}\sum_j e^{i\vec{k}\cdot(\vec{R}_j+\vec{\tau}_\nu)}\varphi_\alpha(\vec{r}-\vec{R}_j-\vec{\tau}_\nu), \tag{21}$$

where $\vec{R}_j$ are the Bravais-lattice vectors and N_3 is the number of Bravais-lattice points in the three-dimensional bulk lattice. The Bloch functions are then expanded as follows:

$$\psi_{n\vec{k}}^0(\vec{r})=\sum_{\alpha\nu}C_{\alpha\nu}^n(\vec{k})\chi_{\vec{k}}^{\alpha\nu}(\vec{r}). \tag{22}$$

Upon diagonalization of the secular matrix $\langle\chi_{\vec{k}}^{\alpha\nu}|H^0|\chi_{\vec{k}}^{\alpha'\nu'}\rangle$ at each $\vec{k}$, one obtains the eigenvalues $E_{n\vec{k}}^0$ and the corresponding eigenvectors $C_{n\vec{k}}^{\alpha\nu}$, which define the Bloch functions. In the applications to be presented in this paper, the matrix elements $\langle\varphi_{\alpha j\nu}|H^0|\varphi_{\alpha' j'\nu'}\rangle$ which are needed to construct $\langle\chi_{\vec{k}}^{\alpha\nu}|H^0|\chi_{\vec{k}}^{\alpha'\nu'}\rangle$ are treated as parameters. The method has often been referred to as the empirical tight-binding method (ETBM).

For an arbitrary perturbation U, one must first choose a basis set in terms of which to expand the new wave functions ψ, express the Green's function G^0, evaluate the matrix of U, and proceed with the formalism described in the previous subsections. In early formulations of the problem, the Wannier functions were thought to be the natural set for localized perturbations. When an LCAO representation is used for the bulk band structure, however, the set of atomic orbitals $\{\varphi_\alpha\}$ has been shown to be a more natural and useful choice for point defects.[60,61] Along the same lines, for planar perturbations, it is natural to use the set $\{\varphi_\alpha\}$ and define *layer*

orbitals in order to take advantage of the fact that the system retains two-dimensional periodicity. Because of this periodicity, a two-dimensional $\vec{q}$ vector is a good quantum number and layer orbitals are simply Bloch sums in two dimensions. They are defined by

$$\Phi_{\vec{q}}^{\alpha m\nu}(\vec{r}) = \frac{1}{\sqrt{N_2}} \sum_j e^{i\vec{q}\cdot(\vec{\rho}_j + \vec{\lambda}_\nu^m)} \varphi_\alpha(\vec{r} - \vec{\rho}_j - \vec{\lambda}_\nu^m) , \tag{23}$$

where $\vec{\rho}_j$ are the lattice vectors of the two-dimensional Bravais lattice and $\vec{\lambda}_\nu^m$ are the position vectors of the atoms in the two-dimensional unit cell. The number of Bravais-lattice points in the two-dimensional lattice is denoted as N_2. The index m labels different planes of atoms and the index ν labels different atoms in the same plane. The above definition of layer orbitals is the same as that used for slab calculations in a LCAO representation. For convenience, we will occasionally use a composite index $l = \alpha m \nu$ for the layer orbitals.

States of the perturbed system are then expanded in terms of the layer orbitals

$$\psi_{s\vec{q}}(\vec{r}) = \sum_l A_{sq}^l \Phi_{\vec{q}}^l(\vec{r}) , \tag{24}$$

where s numbers the various states at each $\vec{q}$. The Green's function G^0 and the perturbation matrix U can then be evaluated in the $\{\Phi_q^l\}$ representation at each $\vec{q}$, from which the determinant $D(E)$, the bound states, the change in the state density $\Delta N(E)$, etc., can be determined.

C. Free surfaces

The next task is to identify the perturbation U describing the creation of a free surface. There are essentially two ways to accomplish this task. One possibility is to "switch off" the interactions (i.e., cut the bonds) between orbitals on the atoms on a number of adjacent planes [Fig. 1a] so that two noninteracting semi-infinite solids are formed. Clearly, the number of planes involved in this procedure is determined by the number of nearest-neighbor interactions that are included in the tight-binding Hamiltonian H^0 of the bulk. For example, if only first-nearest-neighbor interactions are included in the bulk Hamiltonian, switching off the interactions between only two adjacent planes will accomplish the decoupling between the twin surfaces. The interaction between orbital α and orbital β on two different atoms is formally switched off by simply setting $U_{\alpha\beta} = -H^0_{\alpha\beta}$. In this procedure both atoms become involved in the process of creating a surface.

An alternative way to create a free surface is

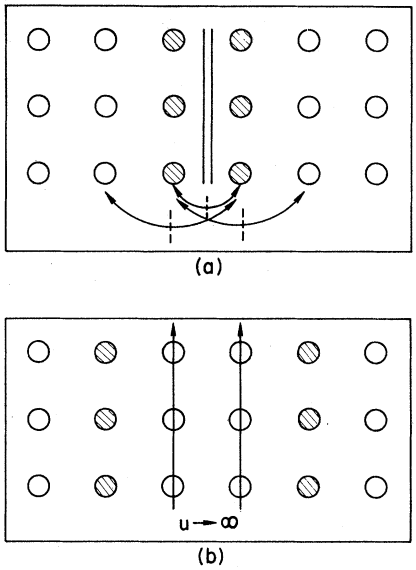

FIG. 3. Schematic graphs showing the creation of the twin surfaces in the two different methods: (a) "bond-cutting" (b) "removal" of layers. In both cases the resulting surface-layer atoms are shaded.

to remove one or more layers of atoms so that again two noninteracting semi-infinite solids are formed [Fig. 1b)]. As it is clear from Fig. 1, the number of planes involved in creating the surface is now smaller (in most cases smaller by a factor of 2). The "removal" of atoms is accomplished by simply setting their diagonal matrix elements to a constant u and then letting that constant go to infinity. (The effective interaction between orbitals on such atoms and orbitals on all other atoms goes to zero as $u \to \infty$). This procedure was used earlier by Bernholc and Pantelides[60] in the case of the vacancy in a bulk semiconductor. In fact, the creation of a surface is equivalent to the introduction of a "planar vacancy" (in the case of nearest-neighbor coupling) or "planar divacancy" (in the case of next-nearest-neighbor coupling), etc. For example, in a one-dimensional crystal with only nearest-neighbor interactions, a vacancy creates two noninteracting semi-infinite solids. Algebraically, the matrix elements of the perturbation U between atomic orbitals α and β are of the form

$$U_{\alpha\beta} = u\delta_{\alpha\beta} , \tag{25}$$

for α and β on the atoms to be removed. With this form of perturbation and in the limit $u \to \infty$, the condition for bound states, Eq. (11), becomes

$$\tilde{D}(E) = \det || G^0_{ll'}(E) || = 0 , \tag{26}$$

where l and l' are layer orbitals on the planes of atoms to be removed. The change in the density

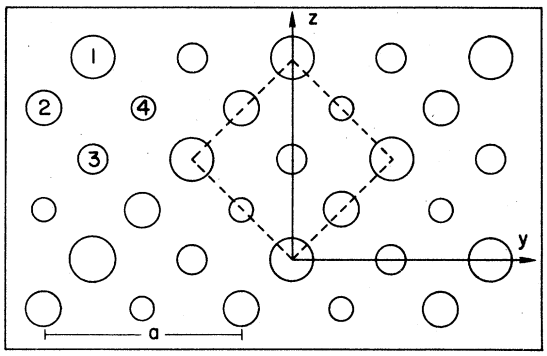

FIG. 2. Topmost (100) surface layer and the following three layers for diamond or zinc-blend lattices. In the case of a zinc-blende material even and odd layers contain either anions or cations, respectively. We retain the crystal y and z axis. The bulk lattice constant is denoted by a.

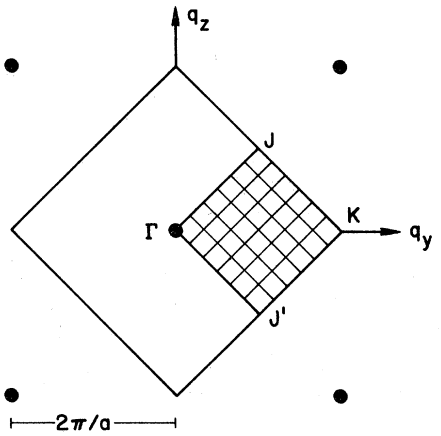

FIG. 3. Reciprocal lattice (dots) for a diamond or zinc-blende (100) surface together with the surface Brillouin zone. The irreducible square (C_{2v} symmetry) is cross-hatched.

of states $\Delta N(E)$ is given by the same expression (15) and (16) with $D(E)$ replaced by $\tilde{D}(E)$ defined by Eq. (26).

The new procedure of creating free surfaces, which we will refer to as the "atom-removal method," has a number of distinct advantages over the previously used method, which we will refer to as the "bond-cutting method." (a) In the bond-cutting method one must set up the Green's-function matrix and the nondiagonal perturbation matrix $U_{l,l'}$, whereas in the atom-removal method it is sufficient to calculate the Green's-function matrix, as can be seen in Eq. (26). This result illustrates that the bulk Green's function contains complete information about the electronic structure of an ideal surface (i.e., no change of the bulk matrix elements up to the surface). (b) Computationally, the dimension of the resultant matrix in the atom-removal method is usually smaller by a factor of 2. (c) The Green's-function matrix G^0 is Hermitian for the bound states, whereas $1 - G^0U$, encountered in the bond-cutting method generally is not. As a result, the atom-removal method reduces the labor at various stages by at least a factor of 4 or 8.

In the above discussion we compared the relative merits of two different ways of constructing the perturbation that creates a free surface in the scattering-theoretical formalism. In either way, the relevant matrices are substantially smaller than the secular matrices encountered in slab calculations. In particular, as will be seen in Sec. III, the secular matrices of typical slab calculations are an order of magnitude larger than our Green's-function matrices.

III. (100) SURFACE OF Si AND Ge— COMPARISON WITH OTHER CALCULATIONS

In this section we present calculations of the electronic structure of the ideal (100) surface of Si and Ge in order to illustrate that calculations using the scattering-theoretical method described above are in fact rather straightforward for real materials and can easily provide a wealth of information.

TABLE I. Tight-binding matrix elements in eV defining the bulk Hamiltonians of the various materials in standard notation. The superscripts (c) and (a) in the headings of the first four columns denote cation and anion, respectively, and the superscripts 1 and 2 in the rest of the columns refer to first- and second-nearest neighbors.

	$E_s^{(c)}$	$E_p^{(c)}$	$E_s^{(a)}$	$E_p^{(a)}$	V_{ss}^1	V_{sp}^1	V_{ps}^1	$V_{pp\sigma}^1$	$V_{pp\pi}^1$	$V_{pp\sigma}^2$	$V_{pp\pi}^2$
Si[a]	−4.203	0.187	···	···	−2.08	2.12	2.12	2.32	−0.52	0.58	−0.10
Ge[a]	−5.830	0.610	···	···	−1.69	2.03	2.03	2.55	−0.67	0.41	−0.08
Ge[b]	−5.75	1.60	···	···	−1.69	2.31	2.31	3.10	−0.95	···	···
GaAs[b]	−3.07	3.47	−8.09	1.28	−1.69	2.37	2.06	3.51	−0.96	···	···
ZnSe[b]	+0.01	6.20	−12.03	1.10	−1.69	2.59	1.07	3.46	−0.75	···	···
SiO_2	13.86	18.36	16.36	−1.77	−1.5	3.76	3.5	5.71	−0.64	···	···
O-O interactions		···	···	···	−0.6	0.8	0.8	1.29	−0.16	···	···

[a] Reference 58.

[b] Reference 65.

The geometrical arrangement of the atoms for the (100) surface of Si is shown in Fig. 2. The axes shown are the crystallographic y and z axis. The two-dimensional unit cell is marked out by the dashed line; it contains one atom in each layer. The corresponding two-dimensional Brillouin zone is shown in Fig. 3. We will use the same ETBM Hamiltonian used by Pandey and Phillips[13,58] to study the (100) surface of Si and Ge so that a direct comparison will be possible. This Hamiltonian uses only s and p orbitals on every atom and retains only first- and some second-nearest-neighbor interactions. The values of the parameters in standard notation are given in Table I. An ideal surface is then defined as an abrupt termination of the bulk crystal, keeping all the intra- and interatomic interactions unaltered. In this approximation, no new parameters are necessary for the calculation of the electronic structure of the free surface. The creation of the surface can be accomplished by removing two layers, as shown in Fig. 4.

A. Energy levels of bound surface states

In the scattering-theoretical method, the first task is the evaluation of the projected band structure (PBS), i.e., the projection of the bulk bands $E_{n\vec{k}}$ with $\vec{k}=(\vec{q}, k_\perp)$ for each $\vec{q}$ in the surface Brillouin zone. The PBS is needed for the calculation of the G^0 matrix (Appendix A), but it is also extremely useful in its own right. It allows one to identify all the gaps and "pockets" where a search must be made in order to determine the positions of states that are truly bound at the surface. We have calculated the PBS for Si(100) and Ge(100) and display them in Figs. 5 and 6. Instead of the usual practice of crosshatching the continuum regions uniformly, we display the actual projected eigenvalues at each $\vec{q}$ for a fixed set of $k_\perp$ values. These are precisely the subset of bulk states which would have to be used if the surface-state wave functions were to be expanded in terms of

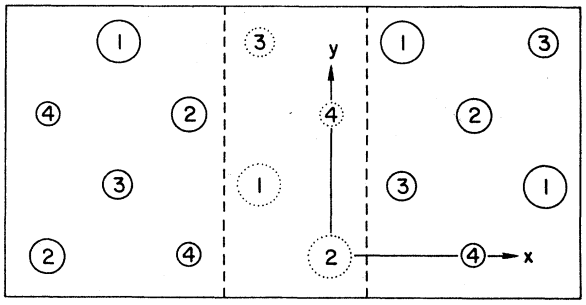

FIG. 4. Geometry in a plane perpendicular to the surface containing the y axis. The two dashed layers are "removed" to create the adjacent surfaces.

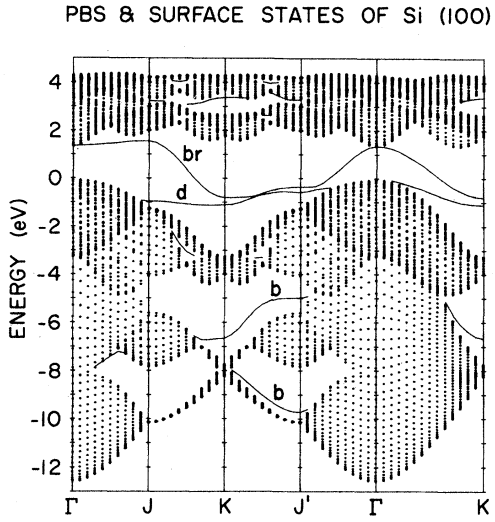

FIG. 5. Projected bulk band structure and surface band structure of Si(100) calculated with the second-nearest-neighbor tight-binding Hamiltonian given in Ref. 58. The letters b, d, and br denote the back-bond, dangling-bond, and bridge-bond bands, respectively. See text.

bulk Bloch functions. The distribution of points at each $\vec{q}$ in Figs. 5 and 6, therefore, provides visual information about which bands contribute more heavily to the formation of surface states. In particular it gives a visual impression of the density of bulk states at each $\vec{q}$.

Bound states in the gaps and pockets of the PBS are determined in an unambiguous way by searching for the zeros of $\tilde{D}_{\vec{q}}(E)$ given by

$$\tilde{D}_{\vec{q}}(E)=\det\left|\left|\langle\Phi_{\vec{q}}^{\alpha m\mu}\left|G^0\right|\Phi_{\vec{q}}^{\alpha' m'\mu'}\rangle\right|\right|, \tag{27}$$

where, for the examples under consideration,

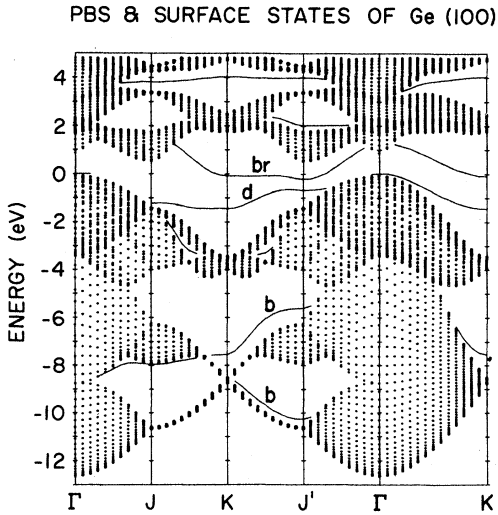

FIG. 6. Surface band structure of Ge(100); for details see caption of Fig. 5.

the indices m and m' run over only the *two* layers that are removed for the creation of the twin non-interacting semi-infinite solids (Fig. 4). The size[63] of the relevant Green's-function matrix is therefore 8×8 and can be evaluated with modest effort (Appendix A). The search for bound states can then be made by using an efficient algorithm described in Appendix B. The results are shown as solid lines in Figs. 5 and 6. We will collectively refer to the surface bands as the surface band structure (SBS).

We turn now to a comparison of the above results with those obtained by Pandey[58] using the slab method in which the semi-infinite solid is simulated by a slab of finite thickness. For the (100) surfaces of Si and Ge Pandey[58] used 20 layers of atoms. The electronic states of the slab were then expanded in terms of layer orbitals and the corresponding secular matrix $\langle \Phi_{\vec{q}}^{\alpha m\mu} | H^0 | \Phi_{\vec{q}}^{\alpha' m'\mu'} \rangle$ was set up and diagonalized at each $\vec{q}$. The size of the slab matrix is thus 80×80, which is an order of magnitude larger than the corresponding scattering-theoretical matrix of Eq. (27). The slab matrix needs of course be diagonalized only once at each $\vec{q}$, instead of at a mesh of energies, and, furthermore, the Hamiltonian matrix elements encountered in the slab method are easier to evaluate than the Green's-function matrix elements. Nevertheless, the scattering-theoretical method is less time consuming if our way of creating the surface is used together with the efficient root-finding algorithm employed in our calculations (see Appendix B). As for the actual results in Figs. 5 and 6, a comparison with the slab calculation shows excellent agreement. For highly localized states the surface-state energies in the case of Si agree within better than 0.01 eV so that there was no reason to plot the slab results separately. In the case of Ge the same agreement is found for most of the states except for a rigid shift[62] of 0.06 eV. (States in the small pockets and the empty states in the conduction band were not reported in Ref. 58.) As one might expect, for extended states there are appreciable differences in the energy positions of surface states. One example is the surface state at Γ in Ge. We find that the state extends over more than 20 layers. Thus, it is not surprising, that the slab-calculation result deviates from our surface-state energy by 0.32 eV. Theoretically, these differences are significant in that we try to solve a given model problem as accurately as possible. Experimentally, extended states are difficult to detect, so that the slab method describes the experimentally interesting states satisfactorily. We will now turn to a discussion of surface-state wave functions.

B. Surface-state wave functions

The calculation of the wave function in our method is rather straightforward, and is described in detail in Appendix C.

In Figs. 7 and 8 we plot orbital sums of the wave-function amplitude on each layer defined by

$$f_{sq}^{m}(E_s)=\sum_{\alpha}\left|\left|A_{s,q}^{m,\alpha}(E_s)\right|\right|^2, \tag{28}$$

for several surface states of Si and Ge. In Fig. 7 we plot for comparison a number of wave functions with distinct behavior. Example 7(a) shows the wave-function amplitude of a gap state which is completely localized in the surface plane. An orbital decomposition of $f_{s,q}^{m}(E)$ shows that this state is 50% p_y- and 50% p_z-like. This type of bond acts like a link between surface atoms and is therefore referred to as the *bridge bond*. The second type of gap states usually encountered on a (100) surface in group-IV semiconductors is the so called *dangling bond*. The wave function corresponding to the dangling-bond state at J is shown in Fig. 7(b). The orbital decomposition of $f_{s,q}^{m}(E)$ for this state shows that it has predominantly s and p_x character, resulting in charge density that "dangles" perpendicular to the surface. A typical example for a *back bond* is given in Fig. 7(c). This state is again very localized,

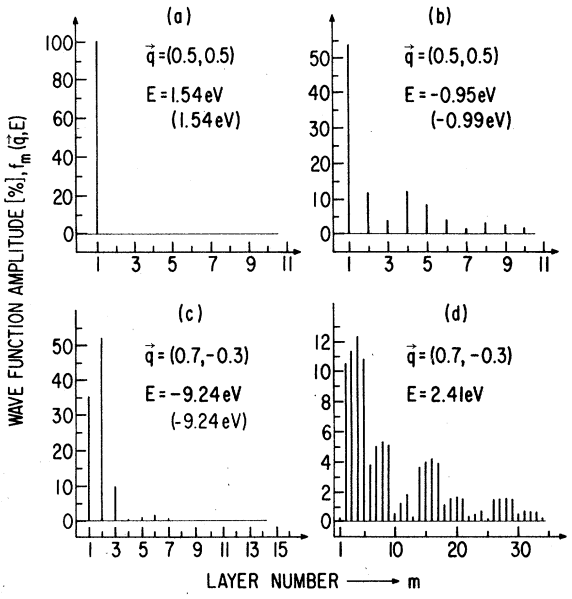

FIG. 7. Wave-function amplitudes as a function of the layer number for some surface states in Si(100) (summed over the s and p orbitals). The corresponding $\vec{q}$ and E values are explicitly given. The energy values resulting from a 20-layer slab calculation (Ref. 58) are also given in parentheses for comparison.

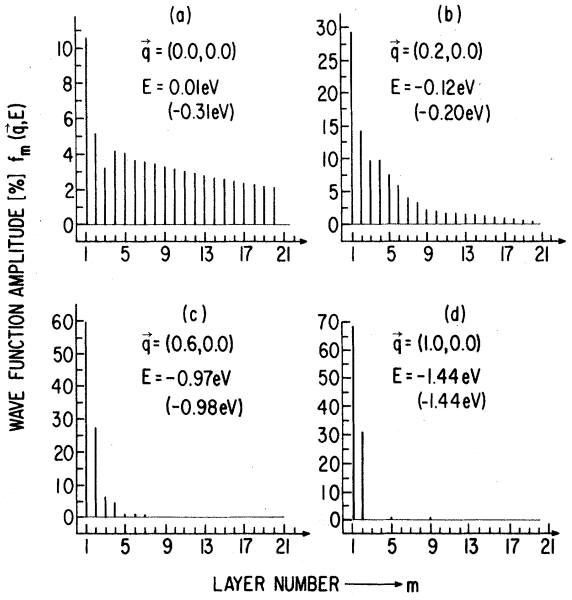

FIG. 8. Wave-function amplitudes for the dangling-bond state of Ge(100); for details see Fig. 7.

but its amplitude is shared mainly by the first two layers indicating a charge buildup in the "back bond." Example 7(d) shows the wave function of an empty state in one of the tiny pockets in the conduction band part of the PBS. Such states lie very near the bulk energy continua and are therefore very extended. Similar states in the valence-band pockets are more localized, but with most of their amplitude on the third to fifth layers.

When a surface-state band approaches the bulk band projection, the states might, depending on the symmetry of their wave functions, become more and more extended. This is shown for the dangling-bond band in Ge between Γ and K in Fig. 8. At K [Fig. 8(d)] the wave function decays within two layers. As the surface band approaches the bulk band projection [Figs. 8(b) and (c)] the wave function becomes more extended and eventually at Γ [Fig. 8(a)] it extends over more than 20 layers.

We have included in Figs. 7 and 8 a comparison between the surface-state energies calculated by our method and by the slab method (energy values in parentheses) for the states whose wave functions we show. For highly localized states [see, e.g., Figs. 7(a), 7(c), 8(c), 8(d)] the energies are exactly the same in the two calculations. For extended states [Figs. 7(b), 8(a), 8(b)] more or less pronounced deviations occur. For such states the slab method would have to employ thicker and thicker slabs. The accuracy of the scattering-theoretical method, remains unaffected by the extent of the wave functions, because it deals with a truly semi-infinite solid. Where the results of the two methods disagree, the scattering-theoretical method is to be viewed as more accurate.

C. Changes in state densities—Surface resonances

In addition to the bound surface states lying within the gaps and pockets of the PBS, the presence of a surface also induces changes in the density of states within the band continua. These changes can be calculated directly by using Eq. (15). For the particular problem at hand we have

$$\Delta\tilde{N}_{\vec{q}}(E)=\frac{1}{\pi}\frac{d}{dE}\tilde{\delta}(E), \tag{29}$$

where

$$\tilde{\delta}_q(E)=-\tan^{-1}[\mathrm{Im}\,\tilde{D}_{\vec{q}}(E)/\mathrm{Re}\,\tilde{D}_{\vec{q}}(E)]. \tag{30}$$

The changes given by Eq. (29), however, apply to the complete "algebraic" system, consisting of two semi-infinite solids and the "removed" layers with states at infinity. In particular, if we define $n_{\vec{q}}^{m}$ to be the new partial density of states for the $m^{\vec{q}\text{th}}$ layer and $n_{\vec{q}}^{0}$ to be the partial density of states for any layer in the infinite bulk crystal, we have

$$\Delta\tilde{N}_{\vec{q}}(E)=\sum_{m}[n_{\vec{q}}^{m}(E)-n_{\vec{q}}^{0}(E)], \tag{31}$$

where the sum is over all the layers, including those removed by the perturbation. For the actual physical system of interest, i.e., a semi-infinite solid, the relevant quantity should not include the removed layers and their states at infinity. Leaving those terms out, we obtain

$$\Delta N_{\vec{q}}(E)=\tfrac{1}{2}[\Delta\tilde{N}_{\vec{q}}(E)+2n_{\vec{q}}^{0}(E)], \tag{32}$$

where the factor of 2 inside the square brackets corresponds to the number of removed layers and the factor of $\frac{1}{2}$ gives the final value for one semi-infinite solid.

Both quantities, i.e., $\Delta\tilde{N}_q(E)$ and $\Delta N_q(E)$, were calculated and found to satisfy Levinson's theorem: $\Delta N_{\vec{q}}(E)$ integrates over the energy range of the bulk bands to -8 corresponding to the eight states at infinity introduced by the atom-removal perturbation and $\Delta N_{\vec{q}}(E)$ integrates to zero. The number of states is thus conserved.

A typical $\Delta N_{\vec{q}}(E)$ for Si at $\vec{q}=(0.5,0.5)(2\pi/a)$ (the J point of the surface Brillouin zone, see Figs. 3 and 5), broadened[64] by 0.1 eV, is given in Fig. 9. If comparison is made with Fig. 5, one observes that the spikes at 1.5 and -1 eV correspond to true surface states in the gap; the remaining structure corresponds to changes in the continuum density of states. Some of the struc-

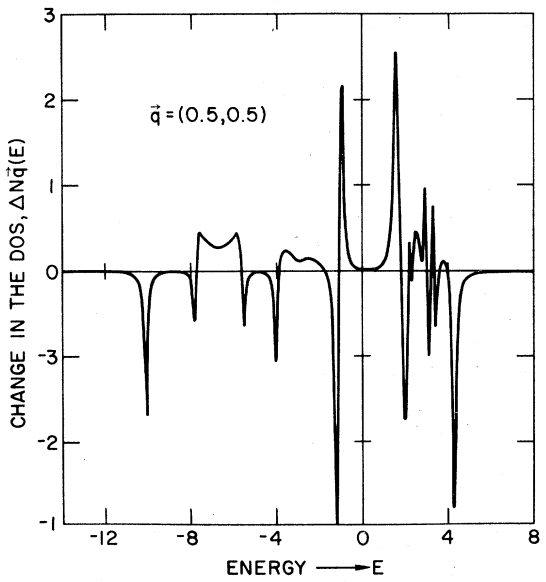

FIG. 9. Total change in the density of states (DOS) at the symmetry point J for Si(100), broadened by 0.1 eV.

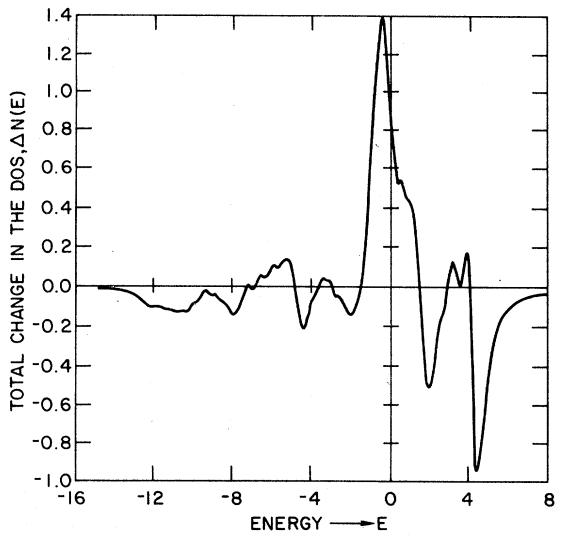

FIG. 10. Total change in the density of states (in units of states/eV unit cell) summed over the surface Brillouin zone for Si(100), broadened by 0.3 eV.

ture can be identified as resonances and antiresonances, as discussed in Sec. II. For example, the negative spikes at −10, −1.2, and 4.3 eV are clearly antiresonances. The structure that appears in the range −8.5−−5 eV looks rather peculiar. At first glance, one might view it as two neighboring resonances giving rise to a twin-peak feature. Such an explanation is not adequate, however, because the integral of $\Delta N_{\vec{q}}(E)$ over this range corresponds only to one extra state. More careful examination reveals that the structure corresponds to two resonances of about the same width *plus* a wider antiresonance between the two. The two negative dips are thus the remnants of the antiresonance tails. Therefore, the net change in the number of states in this energy region should be one, as it was indeed found to be. This structure, therefore, helps demonstrate the fact that the change in the continuum density of states may be considerably more complicated than a mere succession of Lorentzian-type resonances and antiresonances.

If we integrate $\Delta N_q(E)$ of Fig. 9 over the valence bands, i.e., up to about −1 eV (the top of the projected valence bands at J; see Fig. 5), we find that a total of *one* state has been removed. Similarly, if we integrate over the energy range of the projected conduction bands alone, we also find that a total of *one* state has been removed. The two missing states are of course balanced by the two states in the gap, and Levinson's theorem is satisfied. However, the finding also reveals that the two bound states are derived from both the valence and the conduction bands. This realization raises some questions about the validity of a semiempirical Hamiltonian which is chosen to fit the valence bands very well while doing rather poorly for the conduction bands. It is plausible that the lower of the two gap states is determined predominantly by the valence bands and is thus quite reliable, while the upper state is determined by the conduction bands (this point is explored further in Sec. III D below). The most crucial test of a semiempirical surface Hamiltonian is of course a comparison with the surface states obtained by self-consistent calculations, as pursued by Pandey,[58] who concluded that the results were quantitatively accurate.

In Fig. 10 we give the total change in the density of states $\Delta N(E)$, which was obtained by summing over $\vec{q}$ in the surface Brillouin zone. The main features can be understood by referring to Fig. 5. The states in the gap correspond primarily to what we described as the bridge-bond band. The peak at about −0.8 eV corresponds to the dangling-bond band, also shown in Fig. 5. Finally, the extra states at about −6 eV correspond to the surface band that runs from a point near K toward J' in Fig. 5.

We turn now to compare with the slab method once more. By its nature, the slab method is less suitable for the description of changes in the band continua because, unlike the scattering-theoretical method, it simulates the continuum with a set of discrete states. In the case of the (100) surface of Si and Ge discussed here, the 80×80 slab

secular matrix yields 80 energy levels at each $\vec{q}$. A few of these correspond to the bound states in the gaps and pockets discussed earlier. Some of the remaining states which lie within the band continua may be identified as resonances if their wave functions exhibit localization. For example, in Ref. 58 a resonance was found at the J point of Si(100) at -7 eV which is in the middle of the broad structure we discussed earlier (Fig. 9). We found that there are actually two resonances and an antiresonance within that region. It is clear that the procedure of examining slab wave functions is likely to miss both antiresonances and broad resonances. The latter correspond to charge localization building up from small contributions by states over a rather wide energy range.

One procedure that has been used in conjunction with slab calculations is to construct a histogram out of the discrete states. Such histograms for each $\vec{q}$ tend to be rather crude because of the small number of states. They become more meaningful for the total density of states when a sum over $\vec{q}$ is carried out. Note, however, that this procedure yields the total density of states for the perturbed system. One must subtract large similar total state densities for the perturbed and unperturbed systems in order to obtain the small changes due to the perturbation.

D. Local densities of states

In Sec. III C we discussed the total changes in the density of states within the band continua. Those curves contain resonances, antiresonances, and other structure, but convey no information about how localized these features are. What is needed is something analogous to the wave functions of bound states discussed in Sec. III B above. Such information at each $\vec{q}$ vector is contained in *local* densities of states which are defined for each layer by

$$N_l(\vec{q},E) = -(1/\pi)\,\mathrm{Im}\,G_{ll}(\vec{q},E)\,. \tag{33}$$

The calculation of these quantities needs the explicit determination of the new Green's function G in a layer-orbital representation. For this purpose, Dyson's equation [Eq. (13)] must be solved. The procedure is given in detail in Appendix D. Typical results of such calculations are shown in Fig. 11, where $\vec{q}$ was chosen to be (0.5, 0.5), as was the case in Fig. 9. In Fig. 11(a) we display $N_l(\vec{q},E)$ beginning with the surface layer $l=1$ and continuing into the bulk to $l=7$, for which $N_l(\vec{q},E)$ becomes almost identical with the layer density of states in the bulk infinite

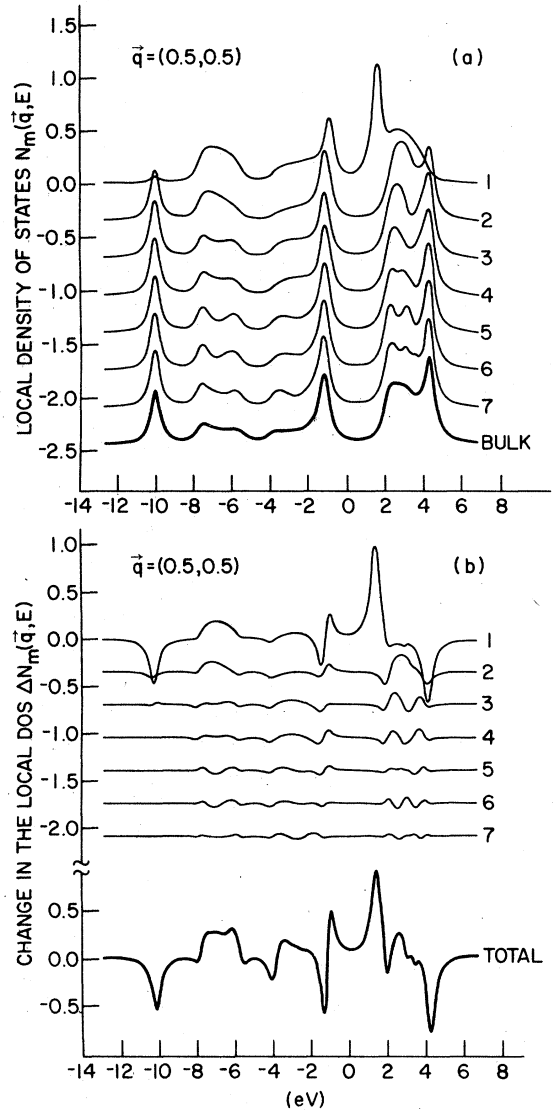

FIG. 11. (a) Local densities of states (in units of states / eV/unit cell) at each one of the first seven layers of the Si(100) surface at the symmetry point J of the surface Brillouin zone. The local density of states at any bulk layer of the infinite crystal is shown by the heavy line. (b) The changes in the local density of states at each of the first seven layers. The total change is given by the heavy line and is the same as that shown in Fig. 9, except for different broadening. All the curves in this figure are broadened by 0.3 eV. The vertical scale applies in (a) and (b) for the first layer only. The other curves are all shifted down by 0.35, 0.7, etc.

crystal. The curves are broadened by 0.3 eV and contain the bound states in the gaps as well. In Fig. 11(b) we display the changes in the local density of states for each layer which illustrate more clearly the decay characteristics of the bound states, the resonances and antiresonances. In particular note that the bound state at 1.54 eV,

whose wave function was shown in Fig. 7(a), is once more seen in Fig. 11 to be localized in the first layer. In contrast, the bound state at −0.9 eV [Fig. 7(b)], is seen in Fig. 11(b) to extend over several layers. We also see in Fig. 11(b) that the prominent antiresonances at about −10 eV is localized within about three layers, whereas the broad feature between −6 and −8 eV, which we discussed in connection with Fig. 9, extends over more than seven layers. Note that for the first two layers, this feature appears to be a single broad resonance at about −7 eV, and was so identified in the slab calculation of Ref. 58. Figure 11 confirms the interpretation of the broad feature as a sum of two resonances and one antiresonance, as discussed Sec. III C above.

In conclusion, we find that the scattering-theoretical method provides a much more direct and accurate description of the changes in the continuum density of states than the procedures used in slab methods.

The Koster-Slater-type scattering-theoretical approach also has advantages over the transfer-matrix method.[42] Both these methods describe truly semi-infinite solids and the labor involved may be comparable. However in the transfer-matrix method one calculates the new Green's function directly, without making use of the unperturbed-crystal solutions, so that *changes* in the electronic structure must be calculated by subtracting two large quantities as in slab techniques. Furthermore the calculation of the surface energy bandstructure in the transfer-matrix method is significantly more laborious as compared to the scattering theoretical approach.

E. Alternate calculation for Ge(100)

In addition to our calculation based on the Pandey-Phillips Hamiltonian for Ge, we have also performed surface-state calculations for Ge(100) using the tight-binding parameters of Chadi.[65] Chadi obtained a good fit to the Ge valence bands with only first-nearest-neighbor interactions (Table I). By comparing our results of the two calculations we are able to arrive at several conclusions about the origins and the nature of the surface states.

The complete PBS and the surface states obtained with Chadi's parameters are given in Fig. 12, which should be compared with Fig. 6. It is clear that the valence-band projections are very similar in the two cases whereas the conduction-band projections are quite different. The first-nearest-neighbor parameters yield a conduction band with a width of 7 eV and its minimum at Γ. The second-nearest-neighbor Hamiltonian yields

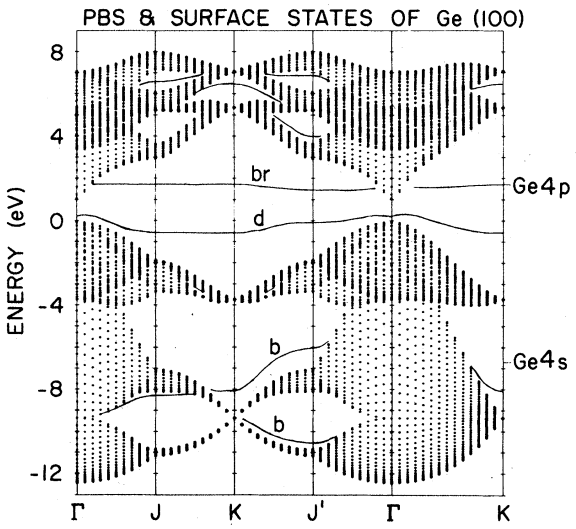

FIG. 12. Projected bulk band structure and surface band structure of Ge(100) calculated with the first-nearest-neighbor tight-binding Hamiltonian as given in Ref. 65. The letters b, d, and br again denote the back-bond, dangling-bond, and bridge-bond bands, respectively. The "atomic" energy levels are shown for convenience. Note that the bridge-bond band is at the $4p$ atomic level in a first-nearest-neighbor approximation.

a conduction band with a width of 3.5 eV and its minimum at the L point (which maps onto J and J'). It is also clear from Figs. 6 and 12 that the surface states obtained in the two cases are qualitatively similar. In the valence bands there is even quantitative agreement in both the energy position and dispersion. The dangling-bond band calculated with the Chadi Hamiltonian is shifted upward by only 0.3 eV, whereas the bridge-bond band is shifted upward by about 1.3 eV with respect to Fig. 6. The width of the bridge-bond band calculated with the first-nearest-neighbor Hamiltonian is smaller (0.3 eV) than the width resulting from the second-nearest-neighbor Hamiltonian (1.45 eV). These results suggest that the dangling-bond band is indeed derived mainly from the valence bands, whereas the bridge-bond band is derived mainly from the conduction bands. It should be noted, that in the first-nearest-neighbor approximation the bridge bond band lies at the atomic-p-level energy. This is a direct consequence of the high localization of the bridge bond and the fact, that neighboring atoms in the (100) plane are second-nearest neighbors.

IV. APPLICATIONS TO OTHER MATERIALS

A. (100) Surfaces of Ge, GaAs, and ZnSe

In this section we apply the scattering-theoretical method to the (100) surfaces of the isoelectronic series Ge, GaAs, and ZnSe. This study

will allow us to address a number of issues that arise in the application of the method to compound semiconductors. The materials were chosen in order to carry out a study of the variation of the surface electronic structure with increasing ionicity. Similar studies of the (110) and the (111) surfaces of this isoelectronic series have been done by others.[66-68]

We again use ETBM Hamiltonians as in Sec. III. For this study of qualitative trends, we use the first-nearest-neighbor Hamiltonians given by Chadi[65] (Table I).

The geometry for the zinc-blende semiconductors is the same as for Si or Ge (Figs. 1–4) except that we have alternate layers of anions and cations. For example, to create a Ga- or an As-terminated surface in GaAs, it is sufficient to remove one As or one Ga layer, respectively. This removal yields a 4×4 Green's-function matrix and creates two inequivalent surfaces.[69] The left-hand semi-infinite solid is rotated about the x-axis by 90° compared to the right-hand semi-infinite solid with respect to their common y-z coordinate system. As a result, the zeros of $\det\|G^0(E)\|$ yield singly degenerate states (except at Γ and K) corresponding to the two surfaces. The states on the two opposite surfaces are related by a simple 90° rotation, so that, e.g., the J point of the one surface corresponds to the J' point of the other, and vice versa. This complication may be avoided by removing two layers, namely, a Ga *and* an As layer. The size of the Green's-function matrix is increased to 8×8, but the energies of the surface states of both Ga- *and* As-terminated (100) surfaces are obtained from the zeros of one determinant. The states of the two surfaces can then be distinguished by either examining the wave functions or, even more simply, by performing a complementary calculation with 4×4 matrices (only one layer removed).

The surface band structure (SBS) for Ge(100), calculated in the first-nearest-neighbor approximation has already been given in Fig. 12 and was discussed in Sec. III D. Our results for the GaAs and the ZnSe (100) surfaces are given in Figs. 13 and 14, where separate plots for the anion- and the cation-terminated surfaces are given.

The first result that is evident from Figs. 13 and 14 is that surface states of an anion-terminated surface tend to be within the valence-band region. Conversely, surface states of a cation-terminated surface tend to be within the conduction bands. This result correlates nicely with the well known fact that bulk valence bands are dominated by anionlike states while conduction bands are dominated by cationlike states (see also Fig. 15). It also demonstrates that the character and energetic position of most surface states depend primarily on the nature of atoms in the first layer.

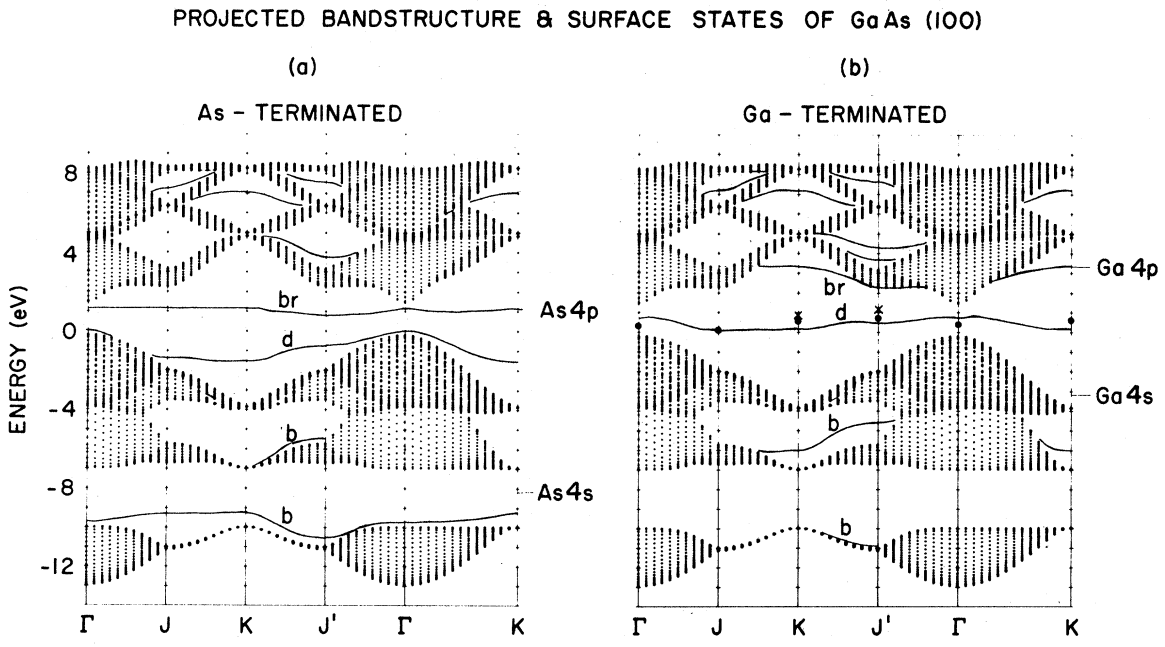

FIG. 13. Surface band structure for the anion- and cation-terminated (100) surfaces of GaAs. For details see Fig. 12. The dots and stars in Fig. 13(b) are the self-consistent results, given in Ref. 28, for the dangling bond and bridge bond, respectively.

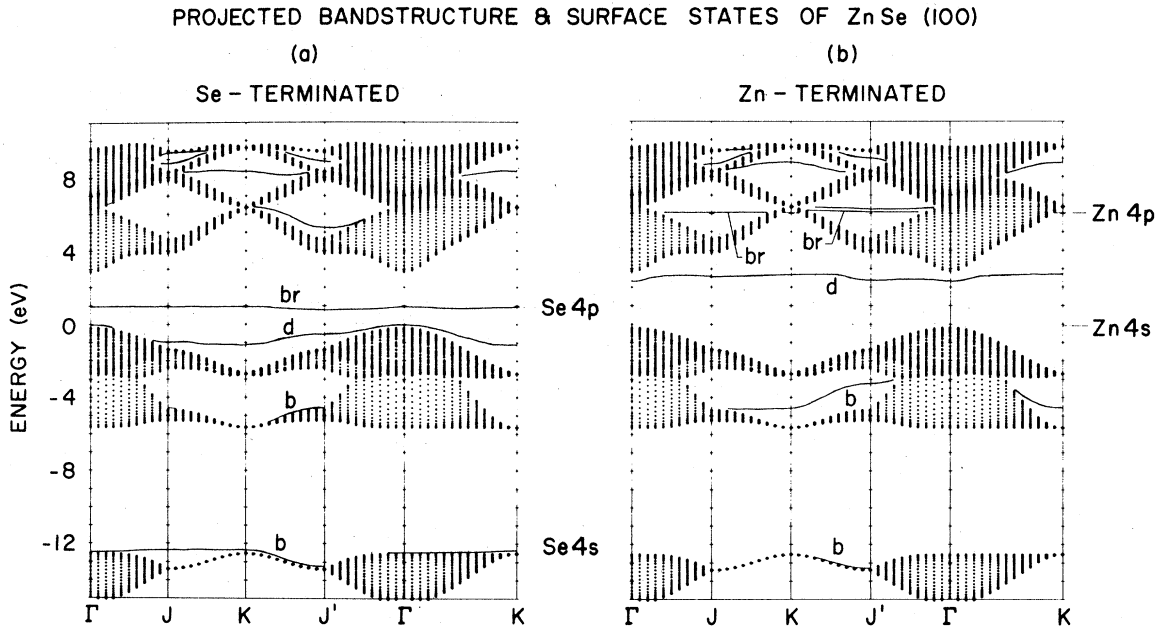

FIG. 14. Surface band structure for the anion- and cation-terminated (100) surfaces of ZnSe. For details see Fig. 12.

If we recall that our ETBM Hamiltonians describe bulk valence bands quite accurately and bulk conduction bands rather poorly, it follows immediately that our calculations of the SBS of the ideal anion-terminated surfaces are quite reliable, whereas the corresponding calculations of the SBS of the ideal cation-terminated surfaces are qualitative at best. We will therefore first discuss anion-terminated surfaces in detail and then make a few remarks about cation-terminated surfaces.

Both GaAs and ZnSe anion-terminated surfaces have a back-bond-type band that lies entirely within the heteropolar gap. These states are highly localized and are predominantly anion s-like, very much like the bulk band immediately below them. These characteristics become more prominent as one goes from GaAs to ZnSe. Similarly, the dispersion of the back-bond-type surface band gets smaller with increasing polarity, as does the dispersion of the bulk band immediately below it.

Both GaAs and ZnSe have another back-bond-type surface state that appears in the pocket around −4 to −6 eV. These states turn out to be more spread out and their dispersion decreases much more slowly along the isoelectronic series.

We turn now to the two surface bands in the fundamental gap. As in the case of Ge, the lower band has a dangling-bond character formed by s and p_x orbitals, whereas the upper band has a bridge-bond p_y-p_z character. In fact, the separation between the bridge bond and the dangling bond may be largely due to the presence of the s admixture in the latter. This is consistent with the fact that the average separation between the two types of states is smaller in ZnSe where the Se atomic s state is lower in energy than in As and thus does not admix as much. As for the dispersion of the two types of states, we note that

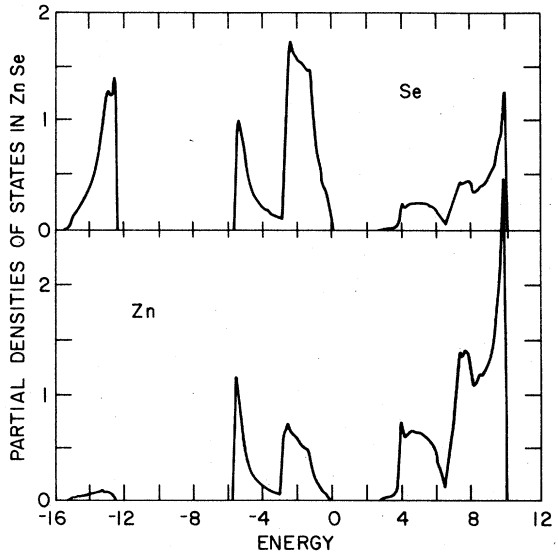

FIG. 15. Partial bulk densities of states at a Se atom (top) and a Zn atom (bottom) for ZnSe calculated with the tight-binding Hamiltonian given in Ref. 65.

the bridge-bond band is almost dispersionless and lies at the atomic p level, whereas the dangling-bond band has more dispersion through interactions mediated by the second layer.

Turning to the cation-terminated surfaces, Figs. 13 and 14 reveal that, qualitatively, a similar set of surface bands is obtained. As noted earlier, the bulk conduction bands are given rather poorly by the ETBM Hamiltonian used in our calculations. The two surface bands within the range of the projected conduction bands are therefore only qualitatively meaningful. The dangling-bond band of GaAs, however, which lies in the fundamental gap appears to agree rather well with the self-consistent results of Appelbaum, Baraff, and Hamann.[28] We investigated the origins of this state at sample $\vec{q}$ points by calculating $\Delta N_{\vec{q}}(E)$ and integrating it over the projected valence bands. The resulting integral was -1 indicating that the state is mainly derived from the valence bands, very much like the dangling-bond band of the (100) surfaces of Si and Ge and the anion-terminated (100) surfaces of GaAs and ZnSe. This finding suggests that the dangling-bond bands even of cation-terminated surfaces can be calculated fairly reliable in a first-nearest-neighbor approximation. Finally, the back-bond states appearing in the valence-band pocket of cation-terminated surfaces (Figs. 13 and 14) are probably derived totally from valence states and are therefore even more reliable.

B. (100) Surface of SiO_2

In this section we study the Si- and the O-terminated (100) surfaces of the ideal cubic form of SiO_2, i.e., β-cristobalite. SiO_2 is an important technological material and is widely used as a substrate for depositing other substances. Knowledge of the surface electronic structure of this material might help understand the way it bonds with other substances. The study we present here is somewhat crude, since we calculate only surface states with the β-cristobalite geometry. On the other hand, studies based on β-cristobalite-like geometries have helped understand most electronic properties of bulk crystalline and amorphous SiO_2. We therefore expect that the present study of SiO_2 surfaces, which is the first to be attempted, will serve as a guide for more

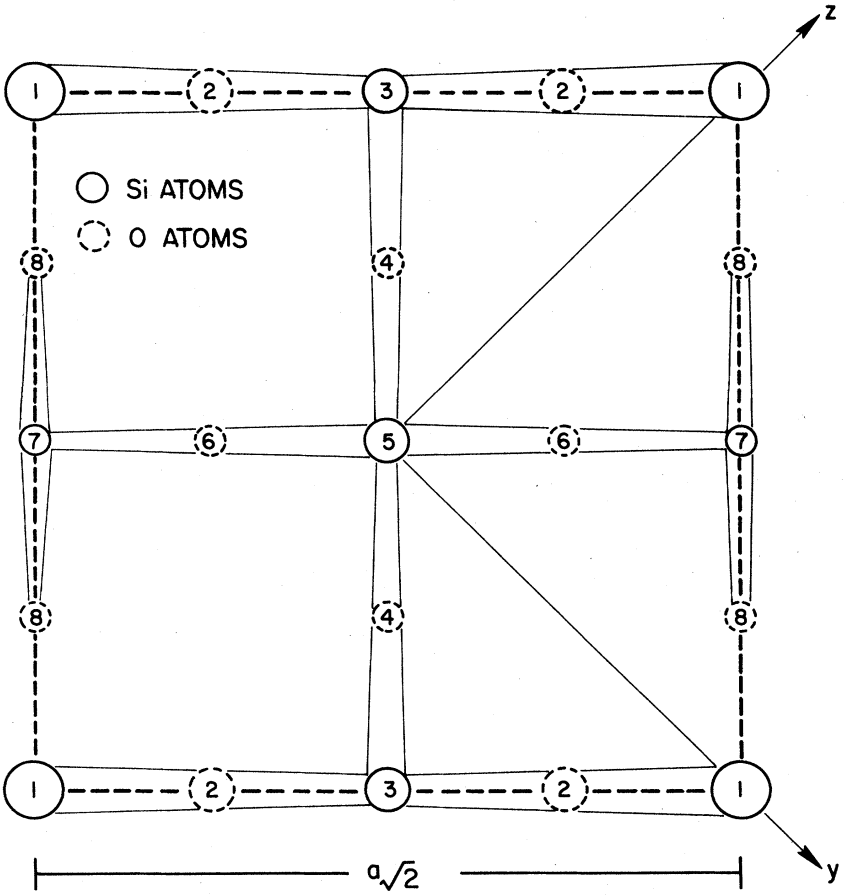

FIG. 16. Topmost (100) surface layer and the following seven layers for the cubic SiO_2 (ideal β-cristobalite) lattice. We again retain the bulk-crystal Cartesian coordinate system. The bulk lattice constant is denoted by a. Si atoms are shown as full and O atoms as dashed circles.

detailed understanding in the future.

The first-nearest-neighbor parameters (Table I) used in the bulk ETBM Hamiltonian, were found by fitting to the SiO_2 bulk valence bands given in Ref. 70 and to a band gap of 9 eV.[71] The valence bands and the band gap are reproduced accurately by retaining only the Si-O and the O-O first-nearest-neighbor matrix elements. The Si-Si interactions are left out. The geometrical arrangement of the atoms for a Si-terminated (100) surface of SiO_2 is shown in Fig. 16, where we have depicted the first eight layers, including the surface layer. The two-dimensional unit cell is again marked by a dashed line. It should be noted, that the unit cell contains one atom in each Si layer but two atoms in each O layer. The point-group symmetry (C_{2v}) and the surface Brillouin zone (SBZ) are the same as in the zinc-blende materials (Fig. 3).

The creation of two adjacent Si-terminated surfaces is accomplished by removing one O layer, yielding an 8×8 Green's-function matrix (two atoms per unit cell). The creation of two adjacent O-terminated surfaces cannot, however, be accomplished by removing only one Si layer, because the resulting two semi-infinite solids are still coupled via the first-nearest-neighbor O-O interactions. In order to accomplish the desired decoupling, at least two layers (one Si and one O layer) must be removed. The result is a 12×12 Green's-function matrix describing one Si-terminated surface and one O-terminated surface. The calculated states can then be sorted by comparing with the previously obtained states for the Si-terminated surface.

The projected valence bands of SiO_2 are shown in Fig. 17. The upper part of the projection, with a width of about 3 eV, results mainly from the nonbonding or "lone pair" O $2p$ orbitals which lie perpendicular to the Si-O-Si chain. The lower part, with a width of about 7 eV, results mainly from the bonding O $2p$ orbitals, which lie along the Si-O-Si chain. The bonding bands have the same overall structure as the valence bands of Si. The similarity in the corresponding parts of the projected band structures may be seen by comparing Figs. 17 and 5.

The surface states for the Si- and O-terminated (100) surfaces of cubic SiO_2 are shown in Figs. 17(a) and 17(b). No bound surface states were found in the optical gap for either surface. The nonbonding bands are affected very little by the creation of the surface. No dangling-bond bands are split off, as expected, because there are no bonds to begin with. Instead, the states in the nonbonding bands are very much atomic in character, so that the creation of the surface is only a weak perturbation, as far as the lone-pair orbitals are concerned. The bonding bands, on the other hand, show pronounced surface states, as one might expect, since bonds are broken by the creation of the surface.

For the Si-terminated surface [Fig. 17(a)] we find a number of surface states which are predominantly localized on the O $2p$ orbitals in the O layer immediately below the surface Si layer. They are therefore best described as back-bond states. The Si dangling-bond states are high in

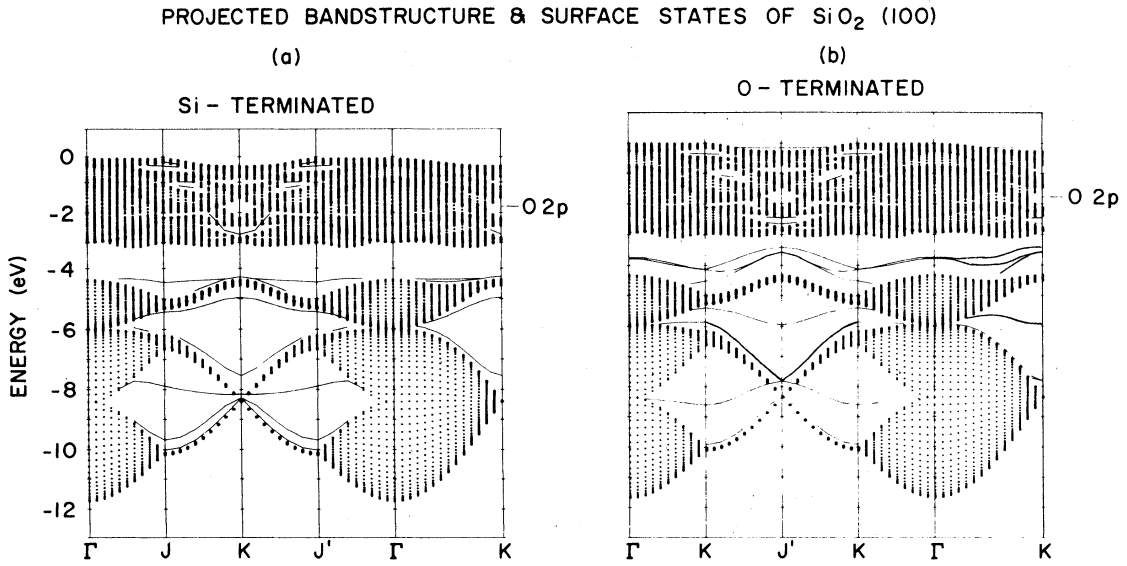

FIG. 17. Projected valence-band and surface band structures for the Si- and O-terminated (100) surfaces of cubic SiO_2. The energetic position of the "atomic" O $2p$ orbitals is indicated.

the conduction bands. Most of the back-bond states lie very close to the bulk band projections and show similar dispersion. This behavior may be explained by the fact that the O atoms in the strengthened back bonds retain all their Si neighbors and four out of their six O neighbors.

In the case of the O-terminated (100) surface [Fig. 17(b)], the perturbation has an even stronger effect. Two of the six O neighbors and one of the two Si neighbors of each surface-layer O atom are removed. The $2p$ orbitals on the surface-layer oxygen atom are, therefore, left dangling, giving rise to two dangling-bond-like bands at around -4 eV in the gap of the PBS between the projection of the nonbonding and the bonding bands. These two dangling-bond bands (resulting from the two atoms in an O layer) are almost degenerate at Γ, but split slightly at other $\vec{q}$ points, because the two $2p$ orbitals point in different directions. Finally, the lower-lying bands have again back-bond character.

The most significant of the above results is the finding that oxygen atoms at the free surface give rise to occupied dangling-bond states which lie in the gap between the bonding and nonbonding valence bands. This finding is independent of our Hamiltonian parametrization and special crystal structure, since the dangling-bond states must lie in the gap[72-75] above the bonding bands and below the nonbonding bands (the energy of a Si–O bond is lower than the energy of an O $2p$ orbital, and the energy of a Si–O–Si bond is even lower). These states should be observable and can probably be detected by high-resolution experiments.

V. CONCLUSIONS

We have demonstrated that the Koster-Slater method for dealing with localized perturbations can be formulated in a way that allows the study of the electronic structure of surfaces of real materials. We have pointed out the various advantages of the method, when used in conjunction with tight-binding Hamiltonians. We illustrated applications of the method to the free (100) surfaces of Si, Ge, GaAs, ZnSe, and cubic SiO_2. The method would be particularly suited for the study of reconstructed surfaces, where large unit cells are involved. Such studies have not been pursued yet. Instead, we have modified the method to treat interfaces between two semi-infinite crystalline solids. This work will be reported in a separate paper. Finally the method has the potential of being a very efficient way of carrying out self-consistent calculations of the electronic structure of surfaces and interfaces.

ACKNOWLEDGMENTS

We are indebted to J. F. Janak for a general program to calculate tight-binding bulk energy bands of arbitrary crystalline materials and to J. Bernholc, J. F. Janak, S. G. Louie, and A. R. Williams for valuable discussions. This work was supported in part by the Office of Naval Research under Contract No. N00014-76-C-0934.

APPENDIX A: EVALUATION OF THE GREEN'S-FUNCTION MATRIX ELEMENTS

The matrix elements of the Green's function $G^0(E)$ [Eq. (3)] in the layer-orbital representation [Eq. (23)] are given by

$$G^0_{l,l'}(E,\vec{q}) = \sum_{n\vec{k}} \frac{\langle l\vec{q}|n\vec{k}\rangle\langle n\vec{k}|l'\vec{q}\rangle}{E^+ - E_n(\vec{k})}\,, \tag{A1}$$

where $|n\vec{k}\rangle$ are the Bloch functions [Eq. (22)] and $|l\vec{q}\rangle$ are the layer orbitals defined by Eq. (23).

In order to evaluate the matrix elements in (A1), we must introduce further notation. We first rewrite the bulk atomic-position vectors in terms of two-dimensional Bravais-lattice vectors $\vec{\rho}_j$ plus appropriate basis vectors in the form

$$\vec{R}_j + \vec{\tau}_v = \vec{\rho}_j + \vec{\lambda}^m_\mu\,. \tag{A2}$$

Furthermore we need to decompose the basis vector $\vec{\lambda}^m_\mu$ into a surface-parallel component $\vec{\sigma}^m_\mu$ and a perpendicular component $\vec{\kappa}^m$:

$$\vec{\lambda}^m_\mu = \vec{\sigma}^m_\mu + \vec{\kappa}^m\,. \tag{A3}$$

Note that for any bulk atom, $\vec{\rho}_j$ locates a two-dimensional Bravais-lattice point, $\vec{\kappa}^m$ locates a particular plane, and finally $\vec{\sigma}^m_\mu$ defines the atomic position in the two-dimensional unit cell in that plane.

Along the same lines, the bulk $\vec{k}$ vector must be decomposed into surface-parallel and -perpendicular components:

$$\vec{k} = (\vec{q}+\vec{g}) + \vec{k}_\perp\,. \tag{A4}$$

Note that the surface-parallel component has been written as the sum of a $\vec{q}$ vector in the SBZ and a two-dimensional reciprocal-lattice vector $\vec{g}$, because the projection of $\vec{k}$ onto the surface does not necessarily lie within the two-dimensional Brillouin zone.

With the above decompositions, the matrix elements appearing in (A1) can be evaluated. The result is

$$G^0_{ll'}(E,\vec{q}) = \frac{N_2}{N_3} \sum_n \sum_{\vec{k}_\perp} \sum_{\vec{g}}{}' \frac{1}{E^+ - E_n(\vec{k}_\perp, \vec{q}+\vec{g})} \times P^n_{ll'}(\vec{k}_\perp, \vec{q}+\vec{g})\,. \tag{A5}$$

The auxiliary function P is given by

$$P^n_{ll'}(\vec{k}_\perp, \vec{q}+\vec{g}) = C^n_{\alpha' m' \mu'}(\vec{k}_\perp, \vec{q}+\vec{g})\, C^{n*}_{\alpha m \mu}(\vec{k}_\perp, \vec{q}+\vec{g}) \times \exp[i\vec{g}\cdot(\vec{\sigma}^m_\mu - \vec{\sigma}^{m'}_{\mu'})] \exp[i\vec{k}_\perp\cdot(\vec{\kappa}^m - \vec{\kappa}^{m'})]. \quad \text{(A6)}$$

Note that the Bloch-function coefficients C now have the double index m, μ in place of the single index ν appearing in Eq. (22) because of the decomposition given in (A2). Finally, the prime on the $\vec{g}$ sum in Eq. (A5) means that the sum is carried out only over those $\vec{g}$ vectors necessary to cover the projection of the bulk Brillouin zone onto the surface as required by the decomposition (A4).

For the (100) surface of a diamond- or zinc-blende-type material, the projection of the bulk Brillouin zone is shown in Fig. 18 together with the SBZ. Also shown is the irreducible segment of the SBZ, marked by the four high-symmetry points Γ, J, J', and K. For $\vec{q}$ vectors inside the crosshatched region of the SBZ, no $\vec{g}$ vectors contribute to the sum in Eq. (A5). For $\vec{q}$ vectors in the remainder of the irreducible square there exist nontrivial contributions to the $\vec{g}$ sum in Eq. (A5). This means that one must sum over $k_\perp = k_x$ both at the $\vec{q}$ point itself and at the corresponding $\vec{q}+\vec{g}$, as shown by the hatched regions in Fig. 18.

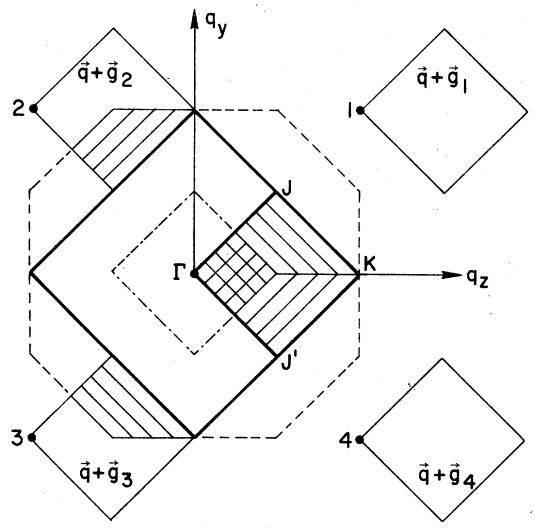

FIG. 18. The dots at Γ and at 1, 2, 3, and 4 are reciprocal-lattice points for the Si (100) surface. The heavy line shows the surface Brillouin zone. The square denoted by Γ, J, K, J' is the irreducible part of the surface Brillouin zone. When $\vec{q}$ runs over this irreducible part, the vectors $\vec{q}+\vec{g}_i$ for $i=1,2,3,4$ ($\vec{g}_i$ being surface reciprocal-lattice vectors) run over the four squares marked by the corresponding $\vec{q}+\vec{g}_i$. The dashed octagon is the projection of the bulk Brillouin zone onto the (100) surface and the dashed-dotted square is the projection of that part of the bulk Brillouin zone, for which $-2\pi/a \leq k_x \leq 2\pi/a$ holds. The details concerning the crosshatched and the shaded areas are discussed in Appendix A.

For $\vec{q}$ points inside the crosshatched region of the SBZ, the sum over $k_\perp = k_x$ extends from $-2\pi/a$ to $+2\pi/a$, where a is the lattice constant, as illustrated for $\vec{q}$ points along the ΓJ line in Fig. 19. The figure is simply the cut of the bulk Brillouin zone by the plane which is perpendicular to the surface and contains the line ΓJ. For $\vec{q}$ points outside the crosshatched region of the irreducible square, the limits at $\vec{q}$ and $\vec{q}+\vec{g}$ are different and $\vec{q}$ dependent, as illustrated in Fig. 19 for one such point q. By making use of symmetry considerations, it can be shown that instead of summing over the appropriate ranges of k_x at both $\vec{q}_0$ and $\vec{q}_0+\vec{g}$, the same result may be obtained by simply summing only at $\vec{q}_0$ over the range $-2\pi/a$ to $2\pi/a$ (Fig. 19). This alternative way of evaluating the sums in Eq. (A5) is a substantial simplification especially for $\vec{q}$ points away from high-symmetry lines in the SBZ.

For the (100) surfaces of diamond- and zinc-blende-type materials, $\kappa^m = \frac{1}{4}am$ and Eqs. (A5)–(A6) simplify to

$$G^0_{ll'}(\vec{q}, E) = \frac{1}{2}\sum_n \int_{-1}^{1} dx\, e^{[i\pi x(m-m')/2]} \times \frac{C^{n*}_{l'}(x,\vec{q})\, C^n_l(x,\vec{q})}{E^+ - E_n(x,\vec{q})}, \quad \text{(A7)}$$

where $x = k_x a/2\pi$. Before this expression can be evaluated, one must deal with the fact that E^+ stands for $E+i\epsilon$, and the limit $\epsilon \to 0$ is to be taken. In the gaps and pockets of the PBS one can simply set $\epsilon = 0$ and evaluate $G^0_{ll'}(\vec{q}, E)$ without any complication, because the denominator in (A7) is

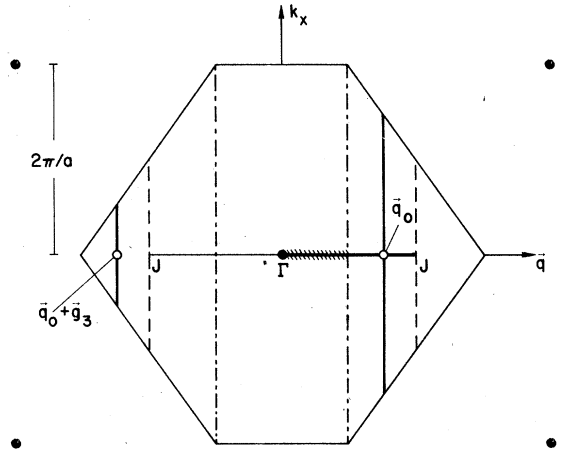

FIG. 19. Cut of the bulk Brillouin zone perpendicular to the (100) surface containing the line J, Γ, J of the surface Brillouin zone. For details see discussion in Appendix A.

never zero. In addition, $G^0_{ll'}$ is Hermitian, which reduces the computational effort even further. Within the PBS continua, however, ϵ cannot be set to zero. There are two ways to proceed: The most direct way is to set ϵ to a small but finite energy and evaluate Eq. (A7) as it stands. The result will be a Green's function which is broadened by the amount ϵ. Alternatively, one introduces the spectral function

$$S_{ll'}(\vec{q},E)=\sum_{n}\sum_{i}\sum_{\vec{g}}{}' P^n_{ll'}(k^i_\perp,\vec{q}+\vec{g})\left(\frac{\partial E_n(k_\perp,\vec{q}+\vec{g})}{\partial k_\perp}\bigg|_{k_\perp=k^i_\perp}\right)^{-1}, \tag{A10}$$

where $k^i_\perp$ are defined by

$$E=E_n(k^i_\perp,\vec{q}+\vec{g}). \tag{A11}$$

For our particular case, the final result for $S_{ll'}$ is $[x_j=k^j_\perp(2\pi/a)]$

$$S_{ll'}(\vec{q},E)=\frac{1}{2}\sum_{j}e^{[i\pi x_j(m-m')/2]}\times\sum_{n}C^{n*}_{l'}(x_j,\vec{q})C^n_l(x_j,\vec{q})\times\left(\frac{\partial E_n(x,\vec{q}+\vec{g})}{\partial_x}\bigg|_{x=x_j}\right)^{-1}, \tag{A12}$$

where x_j is defined by

$$E=E_n(x_j,\vec{q}), \tag{A13}$$

and $-1<x_j<1$.

APPENDIX B: SEARCH FOR THE BOUND-STATE ENERGIES

The energies of bound surface states are determined by the zeros of

$$\tilde{D}(E)=\det\left|\left|G^0_{l,l'}(E,\vec{q})\right|\right|=0, \tag{B1}$$

where l and l' run over the layers which have to be removed for the creation of the surface. (See Appendix A for the evaluation of the matrix $G^0_{l,l'}$.) The determinant in (B1) may be evaluated numerically in a variety of ways but the search for the zeros could be a time-consuming task. Instead, the zeros can be located much more efficiently by first converting the matrix $G^0_{ll'}$, to triangular form and counting the number of negative diagonal elements. If this number is different at the two ends of a given energy range, the difference corresponds to the number of zeros of $\tilde{D}(E)$ in that range. The chosen range is then systematically bisected until the positions of zeros are determined to the desired degree of accuracy. In our calculations the surface states of the chosen Hamiltonians were determined with an accuracy of 1 meV.

$$S_{ll'}(\vec{q},E)=\sum_{n\vec{k}}\langle l\vec{q}\,|\,n\vec{k}\rangle\langle n\vec{k}\,|\,l'\vec{q}\rangle\,\delta(E-E_{n\vec{k}}), \tag{A8}$$

and takes the limit $\epsilon\to 0$ analytically resulting in

$$G^0_{ll'}(\vec{q},E)=\oint\frac{S_{ll'}(\vec{q},E')}{E-E'}dE'-i\pi S_{ll'}(\vec{q},E), \tag{A9}$$

where the bar on the integral sign denotes principal value. $S_{ll'}$ can be evaluated directly. The result is

APPENDIX C: CALCULATION OF THE WAVE FUNCTIONS

The eigenvectors of the Hamiltonian H are given by the Lippmann-Schwinger equation

$$\psi=\varphi+G^0U\psi=\varphi+GU\varphi, \tag{C1}$$

where φ is the solution of H^0, i.e., φ stands in our problem for a bulk Bloch function. In the pockets and gaps of the PBS, where the true surface states are encountered, there exists no nontrivial solution of H^0. Therefore, the wave function for the surface states is given as

$$\psi=G^0U\psi. \tag{C2}$$

In the surface problems discussed in this paper, the perturbation operator acts only on a very limited part of the Hilbert space of H^0, as was extensively discussed in Sec. II. We, therefore, partition the perturbation operator, the Green's operator and the wave function in the two subspaces of H^0, which we label A and B:

$$U=\begin{pmatrix}u1_A & 0\\ 0 & 0\end{pmatrix},\quad G^0=\begin{pmatrix}G^0_{AA} & G^0_{AB}\\ G^0_{BA} & G^0_{BB}\end{pmatrix},\quad \psi=\begin{pmatrix}\psi_A\\ \psi_B\end{pmatrix}, \tag{C3}$$

where 1_A is the unit operator in the subspace A. With (C3) inserted in (C2) we find

$$\psi_A=G^0_{AA}u\psi_A, \tag{C4a}$$

$$\psi_B=G^0_{BA}u\psi_A. \tag{C4b}$$

Equation (C4a) may also be written

$$[(1/u)1_A-G^0_{AA}](u\psi_A)=0. \tag{C5}$$

This is a homogeneous set of linear equations and can be solved for $(u\psi_A)$ for any arbitrary value of u. In the limit $u\to\infty$ one simply diagonalizes

G^0_{AA} and the resulting eigenvectors $u\psi_A$ are finite so that $\psi_A = 0$, as expected. The quantities $u\psi_A$ are then inserted in (C4b) and ψ_B can be directly calculated by simply multiplying the matrix G^0_{BA} by the column vector $(u\psi_A)$.

APPENDIX D: THE SOLUTION OF THE DYSON EQUATION

The formal solution of the Dyson equation (13)

$$G = G^0 + G^0 U G , \tag{D1}$$

can conveniently be written in terms of the scattering matrix

$$T = U(1 - G^0 U)^{-1} , \tag{D2}$$

so that

$$G = G^0 + G^0 T G^0 . \tag{D3}$$

Equation (D3) shows that the complete information about the new features of the perturbed system $H = H^0 + U$ is contained in the scattering-matrix T. Due to the limited range of U, the scattering matrix can be calculated exactly. To calculate T, we have to evaluate $(1 - G^0 U)^{-1}$. We introduce the notation

$$Q = 1 - G^0 U , \tag{D4}$$

and employ the same partitioning convention as in (C3). The matrix Q is of the form

$$Q = \begin{pmatrix} Q_{AA} & 0 \\ Q_{BA} & 1_B \end{pmatrix} , \tag{D5}$$

and can be inverted analytically, even though Q_{BA} and 1_B are infinite submatrices. The result is

$$Q^{-1} = \begin{pmatrix} (Q_{AA})^{-1} & 0 \\ -1_B Q_{BA}(Q_{AA})^{-1} & 1_B \end{pmatrix} . \tag{D6}$$

Using this result we obtain

$$\begin{aligned} G_{AA} &= G^0_{AA} + G^0_{AA} U_{AA} (Q_{AA})^{-1} G^0_{AA} , \\ G_{AB} &= G^0_{AB} + G^0_{AA} U_{AA} (Q_{AA})^{-1} G^0_{AB} , \\ G_{BA} &= G^0_{BA} + G^0_{BA} U_{AA} (Q_{AA})^{-1} G^0_{AA} , \\ G_{BB} &= G^0_{BB} + G^0_{BA} U_{AA} (Q_{AA})^{-1} G^0_{AB} . \end{aligned} \tag{D7}$$

This result holds for any perturbation confined to subspace A. Note that Q_{AA} is precisely the matrix one has to evaluate in order to search for bound states. The complete evaluation of the Green's-function matrix for the perturbed system can then be done directly by inverting the small matrix Q_{AA} and multiplying matrices as required by (D7).

The above results simplify further in the case of the perturbation that creates surfaces used in this paper. The perturbation is of the form

$$U_{AA} = u\, 1_A , \tag{D8}$$

where u is a constant that is eventually let go to infinity. Equation (D7) then becomes

$$\begin{aligned} &G_{AA} = 0, \quad G_{AB} = 0, \quad G_{BA} = 0, \\ &G_{BB} = G^0_{BB} - G^0_{BA}(G^0_{AA})^{-1} G^0_{AB} . \end{aligned} \tag{D9}$$

These equations are valid for all finite energies.[76] Note that $G_{AA} = 0$ corresponds to the fact that there are no states at finite energies in the space occupied by the removed layers. $G_{AB} = 0$ and $G_{BA} = 0$ correspond to the fact that the removed layers are completely decoupled from the two semi-infinite solids described by G_{BB}. It is of particular interest that G_{BB} is given entirely in terms of G^0, which describes the infinite bulk solid. This result is of course true because no electronic or lattice relaxation is included at the surface.

G_{BB} contains a wealth of information. In particular, one can evaluate the local density of states at the lth layer (with l in subspace B) as follows:

$$N_l(\vec{q}, E) = -\frac{1}{\pi} \operatorname{Im}\left(G^0_{ll}(\vec{q}, E) - \sum_{ij} G^0_{li} (G^0_{AA})^{-1}_{ij} G^0_{jl} \right) , \tag{D10}$$

where i and j run over the layer orbitals in the removed layers in the subspace A. The second term in the large parentheses clearly yields directly the change in the local density of states for the lth layer [The sum of these quantities over all layers is equal to $\Delta N(\vec{q}, E)$ discussed in Sec. III.]

---

*Permanent address: Institut für Physik der Universität Dortmund, D-4600 DORTMUND-50, Pf 500 500, West Germany.

[1]V. Heine, Surf. Sci. 2, 1 (1964); Proc. R. Soc. A 331, 307 (1972); The compilation of literature is not intended to be complete, but most of the references to theoretical papers in this field can be found in Refs. 1–55.

[2]See, e.g., *Proceedings of the Second International Conference on Solid Surfaces*, Kyoto, Jpn. J. Appl. Phys. Suppl. 2 (1974).

[3]J. C. Phillips, Surf. Sci. 53, 474 (1975).

[4]J. R. Schrieffer and P. Soven, Phys. Today 28, 24 (1975).

[5]J. A. Appelbaum and D. R. Hamann, Rev. Mod. Phys. 48, 479 (1976).

[6]F. Forstmann, in *Photoemission and the Electronic Properties of Surfaces*, edited by B. Feuerbacher, B. Fitton, and R. F. Willis (Wiley, New York, 1978).

[7]L. P. Batra and O. Roubaux, Surf. Sci. 49, 653 (1975).

[8]G. S. Painter, P. J. Jennings, and R. O. Jones, J. Phys. C 8, L199 (1975).

[9]J. Harris and G. S. Painter, Phys. Rev. Lett. 36, 151 (1976).
[10]I. P. Batra and S. Citraci, Phys. Rev. Lett. 36, 170 (1976).
[11]K. Hirabayashi, J. Phys. Soc. Jpn. 27, 1475, (1969).
[12]Ed Caruthers, L. Kleinmann, and G. P. Alldredge, Phys. Rev. B 8, 4570 (1973).
[13]K. C. Pandey and J. C. Phillips, Phys. Rev. Lett. 32, 1433 (1974); 34, 1450 (1975); Phys. Rev. B 13, 750 (1976).
[14]R. V. Kasowski, Phys. Rev. Lett. 33, 83 (1974); Solid State Commun. 17, 179 (1975).
[15]M. Schlüter, J. R. Chelikowsky, Steven G. Louie, and M. L. Cohen, Phys. Rev. B 12, 4200 (1975).
[16]D. G. Dempsey, L. Kleinman, and Ed Caruthers, Phys. Rev. B 12, 2932 (1975).
[17]K. S. Sohn, D. G. Dempsey, L. Kleinman, and Ed Caruthers, Phys. Rev. B 14, 3185 (1976).
[18]S. Ciraci and I. P. Batra, Solid State Commun. 18, 1149 (1976).
[19]C. Calandra and G. Santoro, J. Vac. Sci. Technol. 13, 773 (1976).
[20]C. M. Bertoni, O. Bisi, C. Calandra, and F. Manghi, Nuovo Cimento B 38, 96 (1977).
[21]O. Bisi and C. Calandra, Nuovo Cimento B 38, 81 (1977).
[22]S. Ciraci and I. P. Batra, Journal 15, 3524 (1977).
[23]I. Ihm, S. G. Louie, and M. L. Cohen, Phys. Rev. B 17, 769 (1978).
[24]G. P. Kerker, S. G. Louie, and M. L. Cohen, Phys. Rev. B 17, 769 (1978).
[25]J. A. Appelbaum and D. R. Hamann, Phys. Rev. B 6, 2166 (1972).
[26]J. A. Appelbaum and D. R. Hamann, Phys. Rev. Lett. 31, 106 (1973).
[27]J. A. Appelbaum, G. A. Baraff, and D. R. Hamann, Phys. Rev. B 11, 3822 (1975).
[28]J. A. Appelbaum, G. A. Baraff, and D. R. Hamann, Phys. Rev. B 14, 1623 (1976).
[29]F. Garcia-Moliner and J. Rubio, J. Phys. C 2, 1789 (1969).
[30]F. Garcia-Moliner, V. Heine, and J. Rubio, J. Phys. C 2, 1797 (1969).
[31]F. Garcia-Moliner and J. Rubio, Proc. R. Soc. A 324, 257 (1971).
[32]F. Flores, Nuovo Cimento B 14, 1, 1973.
[33]M. Elices, F. Flores, E. Louis, and J. Rubio, J. Phys. C 7, 3020 (1974).
[34]J. A. Vergeás and E. Louis, Solid State Commun. 22, 663 (1977).
[35]C. Noguera, D. Spanjaard, and D. W. Jepsen, Phys. Rev. B 17, 607 (1978).
[36]R. Haydock, V. Heine, and M. J. Kelly, J. Phys. C 5, 137 (1972).
[37]R. Haydock and M. J. Kelly, Surf. Sci. 38, 139 (1973).
[38]M. C. Desjonquières and F. Cyrot-Lackmann, J. Phys. B 5, 1368 (1975).
[39]V. Anishchick, L. M. Falicov, and F. Yndurain, Surf. Sci. 57, 375 (1976).
[40]I. B. Ortenburger, S. Ciraci, and I. P. Batra, J. Phys. C 9, 4185 (1976).
[41]E-Ni Foo, M. F. Thorpe, and D. Weaire, Surf. Sci. 57, 323 (1976).
[42]E. J. Mele and J. D. Joannopoulos, Phys. Rev. B 17, 1816 (1978).
[43]J. Koutecky, Phys. Rev. 108, 13 (1957).
[44]J. Koutecky, in *Advances in Chemical Physics* (Interscience, London, 1965), Vol. IX, p. 85.
[45]D. Kalkstein and P. Soven, Surf. Sci. 26, 85, (1971).
[46]A. A. Maradudin, E. Q. Montroll, G. H. Weiss, and I. P. Ipatova, Solid State Phys., edited by F. Ehenreich *et al.* (Academic, New York, 1971), Suppl. 3.
[47]A. van der Avoird, S. P. Liebmann, and D. J. M. Fassaert, Phys. Rev. B 10, 1230 (1974).
[48]S. P. Liebmann, A. van der Avoird, and D. J. M. Fassaert, Phys. Rev. B 11, 1503 (1975).
[49]J. W. Davenport, T. L. Einstein, and J. R. Schrieffer, in Ref. 2.
[50]R. Feder and K. Sturm, Solid State Commun. 14, 1317 (1974); Phys. Rev. B 12, 537 (1975).
[51]V. M. Tapilin, S. L. Cunningham, and W. H. Weinberg, Phys. Rev. B (to be published).
[52]S. L. Weng, Phys. Rev. Lett. 38, 434 (1977).
[53]J. Ladik, Phys. Rev. B 17, 1663 (1978).
[54]N. Lang and W. Kohn, Phys. Rev. B 1, 4555 (1970); 3, 1215 (1971).
[55]N. D. Lang and A. R. Williams, Phys. Rev. Lett. 34, 531 (1975).
[56]J. Callaway, J. Math. Phys. 5, 783 (1964); Phys. Rev. 154, 515 (1967).
[57]F. Garcia-Moliner, in *Theory of Imperfect Crystaline Solids: Trieste Lectures 1970* (International Atomic Energy Agency, Vienna, 1971).
[58]K. C. Pandey, thesis (Columbia University, New York, 1974) (unpublished).
[59]G. F. Koster and J. C. Slater, Phys. Rev. 95, 1167 (1954).
[60]J. Bernholc and S. T. Pantelides, Phys. Rev. B 18, 1780 (1978).
[61]It should be noted that LCAO orbitals are in general not orthogonal and, therefore, present an additional complication over the use of Wannier functions. In the applications discussed in this paper the empirical tight-binding Hamiltonians we use are defined in terms of orthogonal LCAO orbitals (Refs. 13 and 58) so that no complications arise. Use of nonorthogonal orbitals in such schemes results in equations which are modified by the overlap matrix without adding serious complications.
[62]The rigid shift may be due to the definition of the zero of energy in a slab calculation.
[63]The size of the relevant Green's-function matrix is equal to the size of the perturbation matrix. The latter is (number of layers removed) × (number of atoms per layer per two-dimensional unit cell) × (number of orbitals per atom), which in the present case is $2\times1\times4=8$.
[64]The calculations reported here were performed as described in Appendix A by setting ϵ to a small but finite quantity [see discussion following Eq. (A7)]. The corresponding densities are then broadened by ϵ, which is equivalent to convoluting unbroadened curves with Lorentzians of width ϵ. Physically, broadening would arise from lifetime effects and from the measuring process (instrumental broadening) and usually amounts to about 0.5 eV for valence-band states. Most of our calculations were performed with $\epsilon=0.3$ eV, which allowed for speedy calculations and also retained detailed structure in the curves. Only Fig. 9 was computed with $\epsilon=0.1$ in order to illustrate the fine structure present in such curves.
[65]D. J. Chadi, Phys. Rev. B 16, 790 (1977).
[66]J. D. Joannopoulos and Marvin L. Cohen, Phys. Rev. B 10, 5075 (1974).
[67]J. R. Chelikowsky and Marvin L. Cohen, Phys. Rev. B 13, 826 (1976).
[68]D. J. Chadi and Marvin L. Cohen, Phys. Rev. B 11, 732 (1976).
[69]The (100) surfaces in zinc-blende materials are charged

surfaces and are therefore very unlikely to exist in the ideal unrelaxed unreconstructed form.

[70]S. T. Pantelides and W. A. Harrison, Phys. Rev. B 13, 2667 (1976).

[71]T. H. Di Stefano and D. E. Eastman, Solid State Commun 9, 2259 (1971).

[72]Theoretical calculations (Refs. 70, 73–75) find a gap of about 2–3 eV for cubic SiO_2, α-quartz, and amorphous SiO_2. Broadened densities of states show only a dip and agree very well with photoemission data. The presence of the gap is therefore well supported.

[73]J. R. Chelikowsky and M. Schlüter, Phys. Rev. B 15, 4020 (1977).

[74]S. Ciraci and I. P. Batra, Phys. Rev. B 15, 4923 (1977).

[75]P. M. Schneider and W. B. Fowler, Phys. Rev. Lett. 36, 425 (1976).

[76]G_{AA} has poles at infinity corresponding to the states on the removed layers.